Coupling the Xinanjiang model and wavelet-based random forests method for improved daily streamflow simulation

Jian Wang, Weimin Bao, Qianyu Gao, Wei Si and Yiqun Sun

ABSTRACT

Daily streamflow modeling is an important tool for water resources management and flood mitigation. This study compared the performance of the Xinanjiang (XAJ) model and random forests (RF) method in a daily streamflow simulation, and proposed several hybrid models based on the XAJ model, wavelet analysis, and RF method (including XAJ-RF model, WRF model, and XAJ-WRF model). The proposed methods were applied to Shiquan station, located in the Upper Han River basin in China. Five performance measures (NSE, RMSE, PBIAS, MAE, and R) were adopted to evaluate the modeling accuracy. Results showed that XAJ-RF model had a relatively higher level of accuracy than that of the XAJ model and the RF model. Compared to the RF and XAJ-RF models, the performance statistics of WRF and XAJ-WRF were better. The results indicated that the coupled XAJ-RF model can be effectively applied and provide a useful alternative for daily streamflow modeling and the application of wavelet analysis contributed to the increasing accuracy of streamflow modeling. Moreover, 14 wavelet functions from various families were tested to analyze the impact of various mother wavelets on the XAJ-WRF model.

Key words | daily streamflow simulation, hybrid approach, random forests model, wavelet analysis, Xinanjiang model

Jian Wang (corresponding author)
Weimin Bao
Qianyu Gao
Wei Si
Yiqun Sun
College of Hydrology and Water Resources,
Hohai University,
Nanjing 210098,
China
E-mail: *hhuwj2016@163.com*

HIGHLIGHTS

- This study proposed several hybrid models based on the Xinanjiang (XAJ) model, wavelet analysis and the random forests (RF) method (XAJ-RF, WRF and XAJ-WRF model).
- The results indicated that the XAJ-RF model can provide a useful alternative and the application of wavelet analysis contributed to the increasing accuracy in streamflow modeling.

INTRODUCTION

Daily streamflow modeling is an important issue for flood mitigation, drought modeling, and water resources management. It can help urban planners and water-related authorities in better and optimal decision-making (Noori & Kalin 2016). In general, hydrological modeling techniques can be divided into three categories: deterministic distributed models (white box models), conceptual hydrological models (grey box models), and data-driven models (black box models) (Brath *et al.* 2002; Zhang *et al.* 2018). Each kind of model has its own merits and drawbacks.

Both of the former two models are theory driven (Babovic 2005; Rezaie-Balf *et al.* 2017) and they can capture dominant catchment dynamics and describe hydrological sub-processes by mathematical formulas (Kavetski *et al.* 2006). In the deterministic distributed models like MIKE SHE and SWAT,

doi: 10.2166/hydro.2021.111

various hydrological processes of the hydrological cycle can be integrated, considered, and simulated based on partial differential equations of conservation of mess, energy, and motion (Feyen *et al.* 2000). Compared to conceptual models, these models have the obvious advantage of well representing the spatial variability of the underlying surface and precipitation. However, they require a high temporal and spatial resolution of topography, precipitation, evapotranspiration, and other inputs, which have a direct impact on modeling results. The conceptual models like TANK, HBV, XAJ, use simple mathematical elements such as linear or nonlinear reservoirs and channels to describe the hydrological response in an approximate way (Chadalawada *et al.* 2017). Such models involve a limited number of parameters and are commonly used in practice. The Xinanjiang model (XAJ) is one of the most widely applied models since its development in the 1970s, especially in China (Zhao 1977). It is based on the concept of soil moisture replenishment, depletion, and redistribution mechanism, and runs with a smaller number of physically meaningful parameters (Ahirwar *et al.* 2018). In the past decades, many efforts have been directed in the field of the XAJ model and most of them have focused on model calibration (Cheng *et al.* 2006; Xu *et al.* 2013; Tian *et al.* 2019), model improvements (Jayawardena & Zhou 2000; Yao *et al.* 2012; Meng *et al.* 2018), and application in ungauged basins (Li *et al.* 2009; Yao *et al.* 2014; Bai *et al.* 2016). Gan & Biftu (1996) compared the XAJ model with the Nedbor-Afstromnings model (NAM), the Sacramento model (SMA), and the soil moisture and accounting model (SMAR) in eight catchments from different parts of the world. They concluded that XAJ seemed more versatile than other models in handling various catchment conditions because it considered the uneven distribution of runoff producing area. The XAJ model was employed by Jiang *et al.* (2007) for streamflow simulations in the Pearl River basin with good results. Nghi *et al.* (2008) presented hydrological simulations for the Nong Son catchment in central Vietnam with NAM and XAJ models. Their results showed that the XAJ model performed better reproduction of the runoff components. Rahman & Lu (2015) investigated some primary factors affecting spin-up time using the XAJ model for 22 river basins throughout the US. Based on historical climate data and two future precipitation scenarios, Yuan *et al.* (2016) used the XAJ model for streamflow simulation in the Pearl River basin, China. Ahirwar *et al.* (2018) investigated the performance of the Xinanjiang model for runoff simulation in six Indian watersheds having different climatic conditions (dry, average, and wet). Their results indicated the suitability of the XAJ model in wet and average catchment but poor in dry climate areas.

With an increase of computation capability and data availability, the data-driven models are more appealing in the field of streamflow modeling. Different to the former two approaches, the data-driven models build a functional relationship between input and output variables directly without considering the internal structure of underlying physical processes (Solomatine & Ostfeld 2008; Chadalawada *et al.* 2017). These models include traditional statistical techniques such as autoregressive moving average (ARMA) and emerging machine learning methods such as multivariate adaptive regression spline (MARS) (Najafzadeh & Ghaemi 2019; Sadeghi *et al.* 2019; Najafzadeh & Oliveto 2020), genetic programming (GP) (Liong *et al.* 2002; Meshgi *et al.* 2015), model tree (MT) (Homaei & Najafzadeh 2020), chaos theory (Sun *et al.* 2010; Liang *et al.* 2019), wavelet-based neural network (Nourani & Parhizkar 2013; Zeinolabedini & Najafzadeh 2019), and support vector machine (SVM) (Yu *et al.* 2004; Mehrparvar & Asghari 2018). The random forests (RF) model is one of the most commonly used machine learning methods that handles nonlinear and non-Gaussian data well. It is amenable to model interpretation and is free of over-fitting problems as the number of trees increases (Li *et al.* 2016). Wang *et al.* (2015) proposed a flood hazard risk assessment method based on RF and applied it in the Dongjiang River basin, China. Muñoz *et al.* (2018) developed several RF models to forecast discharge based on past precipitation and discharge information. Papacharalampous & Tyralis (2018) assessed the performance of RF and Prophet in forecasting daily streamflow up to 7 days ahead in a river in the US, pointing out that the former model worked better. Li *et al.* (2019) compared the accuracy of five data-driven models (ELM, ELM-kernel, RF, BPNN, and SVR) and found that the RF model was slightly superior to other models in modeling the peak flows.

As a whole, the conceptual hydrological models are limited to simplified hydrological processes and have difficulty coping with complex nonlinear relationships between environmental variables and runoff (Ren *et al.* 2018). However, data-driven models have good capability in capturing complex nonlinear relationships, which can compensate

for the former models. The drawback of data-driven models lies in their overdependence on data and lack of consideration in physical mechanisms. To overcome the aforementioned drawbacks, there is a need to explore the continuum between theory-based and data-driven models, where both theory and data are used in a synergistic manner (Napolitano *et al.* 2009; Karpatne *et al.* 2017). Hybrid models have been investigated in water-related fields, such as modeling flow of waste water pipe (Zoran *et al.* 2003), error updating of numerical models (Babovic *et al.* 2001), and reference evapotranspiration estimation (Raza *et al.* 2020). However, studies of hybrid models in streamflow modeling are limited so far (Babovic 2009; Corzo & Solomatine 2014; Chadalawada *et al.* 2017; Ren *et al.* 2018). Humphrey *et al.* (2016) used the simulated soil moisture from GR4 J model to represent initial catchment conditions in a Bayesian artificial neural network (ANN) model. Noori & Kalin (2016) established a coupled SWAT and ANN model for enhanced daily streamflow prediction, achieving good results. More recently, Chadalawada *et al.* (2020) presented a novel machine learning algorithm guided through the incorporation of existing hydrological knowledge and evaluated the capabilities of the proposed hydrologically informed machine learning framework on the Blackwater River basin in the US. Ghaith *et al.* (2020) proposed a hybrid hydrological data-driven model and found it succeeded in improving daily streamflow prediction compared to HYMOD model. To the best of the authors' knowledge, few works have compared the performance of the XAJ model and wavelet-based RF model (WRF) and the combination of XAJ model and WRF model for daily streamflow simulation has not been reported. In this paper, a hybrid approach of conceptual hydrological model (XAJ model) and random forest method (RF) was developed to improve the daily streamflow simulation in the upper Han River basin, China. Moreover, discrete wavelet transformation technique was further applied to improve the modeling accuracy.

The rest of the paper is organized as follows. The next section describes the Xinanjiang model, RF method, and the proposed hybrid methods. This is followed by a section introducing the study area and data collection. Next, a case study of the daily streamflow simulation and analysis of the modeling results is presented. In the final section, the conclusions are summarized.

METHODOLOGY

In this paper, five models were developed for daily streamflow modeling: (1) Xinanjiang model (XAJ); (2) random forests model (RF) with the inputs of accumulated precipitation and antecedent streamflow; (3) hybrid model (XAJ-RF) with the inputs of antecedent streamflow and simulated streamflow from the XAJ model; (4) wavelet-based RF model (WRF) using subseries of accumulated precipitation and antecedent streamflow as input variables; and (5) hybrid XAJ-WRF model using subseries of antecedent streamflow and simulated streamflow from the XAJ model as input variables. The first two were established as benchmark models for the third hybrid model, while the last two models adopted wavelet transformation technique to further improve the level of accuracy.

Xinanjiang model

The Xinanjiang model is a lumped rainfall-runoff model developed by Zhao *et al.* (1980). The core of this model is the concept of runoff formation on repletion of storage. That is to say, the runoff is not generated until the soil moisture content of the aeration zone reaches field capacity, and thereafter runoff equals the rainfall excess without future loss (Zhao *et al.* 1980). The model consists of four parts as shown in the list below: a three-layer evapotranspiration sub-model, a runoff production sub-model, a runoff separation sub-model, and a runoff concentration sub-model (Figure 1). The inputs are daily precipitation (P) and measured evapotranspiration (EM), and the output is daily streamflow (Q). More details about the XAJ model can be found in Zhao (1992).

1. Evapotranspiration sub-model. This module considers the soil as three vertical layers (upper, lower, and deep layers). The actual evapotranspiration is calculated from potential evapotranspiration while soil storage deficit is calculated in the three-layer soil moisture model (Yao *et al.* 2014).
2. Runoff production sub-model. The module introduced a tension water capacity curve to describe the uneven distribution of tension water capacity throughout the catchment. Runoff is produced once the tension water storage reaches the repletion point.

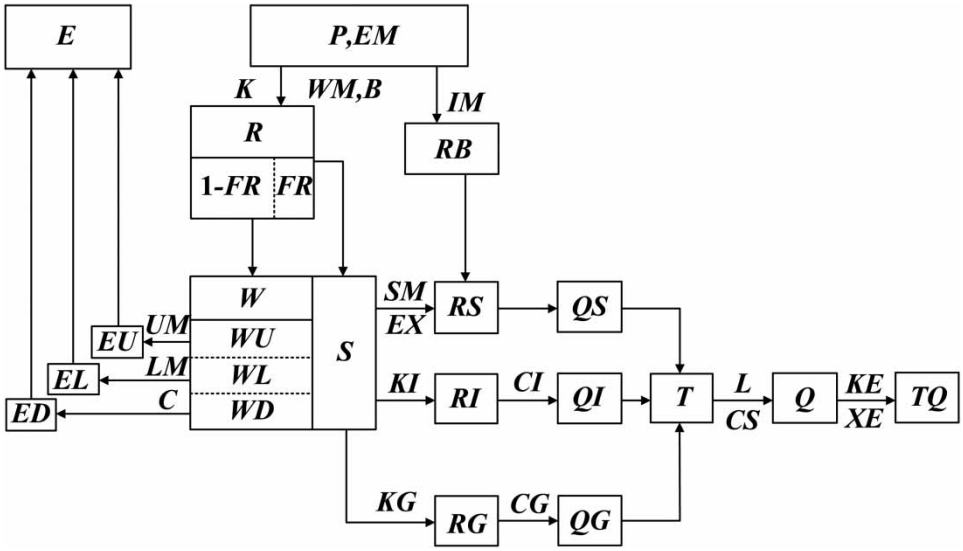

Figure 1 | Flow chart for the XAJ model (adopted from Zhao 1992).

3. Runoff separation sub-model. The total runoff is separated into its three components: surface runoff, interflow, and groundwater according to different free-water storage structure.
4. Runoff concentration sub-model. The surface runoff directly flows into the outlet of the river, while the interflow and groundwater are routed to river channels through linear reservoirs. The discharge of sub-basins flowing to the outlet of the basin can be calculated by Muskingum routing equation.

Random forests

The RF model, proposed by Breiman (2001), is a classification and regression method based on an ensemble of decision trees. The model employs two powerful machine learning techniques: bagging and random feature selection, which are helpful to reduce over-fitting and statistical instability.

Given a training dataset $X_{N\times M}$ (N records with M features), the RF model grows individual classification and regression trees (CART) by randomly selecting S bootstrap samples of size N (the same size as the training dataset) with replacements (Zhu & Pierskalla 2016). Generally, each bootstrap sample leaves out about one-third of the training data, which are also called the out-of-bag (OOB) observations (Xu & Valocchi 2015). The random selection from the features of the dataset is also performed by the selection of m ($m < M$) features as a subset; however, the parameter m is not sensitive to the final output. According to the random subspace theory, the number of selected attributes m was generally determined as the square of the number of input variables M (Liang *et al.* 2017). Therefore, the samples of size N with M features were randomly selected to build a single decision tree. After a large number of trees is generated, the prediction for a new data x is formed by taking the average over the trees, which is also reckoned as ensemble learning.

In this paper, the accumulated precipitation and antecedent streamflow of past 1 days, 2 days, 3 days, and 4 days ($\sum_{t-1}^{t} p_t$, $\sum_{t-2}^{t} p_t$, $\sum_{t-3}^{t} p_t$, $\sum_{t-4}^{t} p_t, Q_{t-1}, Q_{t-2}, Q_{t-3}, Q_{t-4}$) were used as possible inputs to the RF model for daily streamflow simulation. The RF model is easy to tune and implement due to the low number of parameters (Papacharalampous & Tyralis 2018). The main parameter is the number of trees. Higher number of trees always results in more precise predictions but costs more computation time at the same time. Considering the balance between accuracy and computational cost, previous studies found that for most datasets, when the number of trees is 100, the RF accuracy can meet the requirement of the method (Papacharalampous & Tyralis 2018). Thus, S in this research is selected as 100 and the parameter setting remains unchanged in the models involved in

the RF method. More details of the RF model can be found in Xu & Valocchi (2015) and Schnier & Cai (2014).

Wavelet transformation

Conventional rainfall-runoff schemes often use hydrological time series data to approximate the dynamic behavior of the hydrological system. In fact, it is difficult to extract the internal mechanism of rainfall-runoff response based on the one-dimensional series because they are controlled and influenced by complex factors (Chou 2013). In recent years, wavelet-based multi-resolution analysis has been widely used to model a hydrological system at various scales.

Wavelet analysis is an effective tool that provides a temporal representation of the time series. It is performed by wavelet transformation or decomposition that can separate a time series into several components, such as approximation series and detail series. There are two kinds of wavelet transforms: the continuous wavelet transform (CWT) and the discrete wavelet transform (DWT). CWT operates on smooth continuous functions and DWT operates on series that have discrete numbers with Mallat or à trous algorithms (Rathinasamy *et al.* 2015). Given a discrete time series $f(t)$, the CWT and DWT can be expressed as follows (Najafzadeh & Zeinolabedini 2018):

$$W_x(a, b, \psi) = \int_{-\infty}^{+\infty} \frac{1}{\sqrt{a}} f(t)\psi * \left(\frac{t-b}{a}\right) dt \quad (1)$$

$$W_x(a, b, \psi) = a_0^{-\frac{m}{2}} \int_{-\infty}^{+\infty} f(t)\psi * (a_0^{-m}t - nb_0)dt \quad (2)$$

where * is indicative of complex conjugate function, $\psi(t)$ is the mother wavelet, m and n are integer values, a and b are the frequency factor and time factor, respectively. The signal f can be decomposed to a low frequency part a_1 and a high frequency part d_1 at level 1, that is, $f = a_1 + d_1$ (Kisi & Shiri 2011). Similar operations can be performed to decompose the series to finer scales. In previous studies, the decomposition level has be obtained using the following equation:

$$L = \text{int}(\log(N)) \quad (3)$$

where L denotes the decomposition level, N denotes the total number of time series and int() represents the integer-part function. In this paper, the L value was determined to 3 according to the used datasets. Consequently, the hydrological series was decomposed to four subseries components (a_3, d_1, d_2, and d_3).

Hybrid models

To improve daily streamflow simulation, three hybrid models (XAJ-RF, WRF, and XAJ-WRF) were developed based on the Xinanjiang model, wavelet analysis, and random forests model. In the XAJ-RF model, two input variables, the antecedent streamflow with the highest correlation coefficient and the simulated streamflow from the XAJ model, were used as inputs to the RF model for daily streamflow simulation. In the WRF model, the accumulated precipitation and antecedent streamflow term with the highest correlation coefficient were decomposed by various mother wavelets; thus, eight subseries acted as input variables to the RF model. Compared to the WRF model, the accumulated precipitation was replaced by the simulated streamflow from the XAJ model in the XAJ-WRF model. The input variables of the RF model and hybrid models are shown in Table 1.

Performance measures

The efficiency of the models was evaluated based on several commonly used statistics: Nash–Sutcliffe efficiency

Table 1 | Input variables of RF model and hybrid models.

Models	aP	aS	Sxaj	wP	wS	wSxaj
RF	√	√				
XAJ-RF		√	√			
WRF				√	√	
XAJ-WRF					√	√

aP: accumulated precipitation; aS: antecedent streamflow; Sxaj: simulated streamflow by XAJ; wP: subseries of accumulated precipitation obtained by wavelet analysis; wS: subseries of antecedent streamflow obtained by wavelet analysis; wSxaj: subseries of simulated streamflow by XAJ obtained by wavelet analysis.

coefficient (NSE), root mean squared error (RMSE), percent bias (PBIAS), mean absolute error (MAE), and correlation coefficient (R). The optimal value of NSE, RMSE, and PBIAS are 1, 0, and 0, respectively. The lower value of RMSE indicates the higher accuracy of the model. MAE describes the average magnitude of the simulation errors and R describes the degree of collinearity between observations and simulations (Moriasi *et al.* 2007).

$$NSE = 1 - \frac{\sum_{t=1}^{T}(O_t - S_t)^2}{\sum_{t=1}^{T}(O_t - \overline{O})^2} \tag{4}$$

$$RMSE = \sqrt{\frac{1}{T}\sum_{t=1}^{T}(O_t - S_t)^2} \tag{5}$$

$$PBIAS = \frac{\sum_{t=1}^{T}(O_t - S_t) * 100}{\sum_{t=1}^{T}(O_t)} \tag{6}$$

$$MAE = \frac{1}{T}\sum_{t=1}^{T}|O_t - S_t| \tag{7}$$

$$r = \frac{\sum_{t=1}^{T}(O_t - \overline{O})(S_t - \overline{S})}{\sqrt{\sum_{t=1}^{T}(O_t - \overline{O})^2}\sqrt{\sum_{t=1}^{T}(S_t - \overline{S})^2}} \tag{8}$$

where O_t represents the observed streamflow, S_t represents the simulated streamflow, $\overline{O}$ denotes the mean of observed streamflow, and T denotes the total number of observations. Moreover, the Fisher test (F-test) uses the F ratio to assess the hypothesis asserting that the variance term expressed by the model is higher than the variance expressed by the averages; the details of F-test can be found in Najafzadeh & Kargar (2019). According to previous research that has provided some guidelines for daily streamflow evaluation (Moriasi *et al.* 2007; Noori & Kalin 2016; Chadalawada & Babovic 2019), the following ratings were adopted in this study:

Very good: $NSE \geq 0.75$; $PBIAS \leq 0.25$
Good: $0.65 \leq NSE < 0.75$; $0.25 < PBIAS \leq 0.5$
Satisfactory: $0.5 \leq NSE < 0.65$; $0.5 < PBIAS \leq 0.7$
Unsatisfactory: $NSE < 0.5$; $PBIAS > 0.7$

Moreover, the Fisher test (F-test) uses the F ratio to assess the hypothesis asserting that the variance term expressed by the model is higher than the variance expressed by the averages (Najafzadeh & Kargar 2019). The F-test claims that null hypothesis is accepted if $F_0 > F_{\alpha,k,n-p}$, where α represents the significant level; k represents the number of independent variables and $p = k + 1$; n represents the size of the data sample. Generally, the values of α, k and $n - p$ are fixed to 0.05, 6, and 49, respectively. According to the F distribution table, $F_{0.05,6,49}$ is 2.295. Moreover, F_0 is computed as follows:

$$F_0 = \frac{n-p}{k} \cdot \frac{\sum_{t=1}^{T}(S_t - O_t)^2}{\sum_{t=1}^{T}(S_t - \overline{O})^2} \tag{9}$$

STUDY AREA AND DATA

Han River originates in the Qinling Mountains in Shanxi Province and joins the Yangtze River at Wuhan City in Hubei Province, with a total length of 1,577 km. It is the largest tributary of the Yangtze River and covers a total area of approximately 159,000 km^2. The Han River basin belongs to the subtropical monsoon climate zone of East Asia. It is worth noting that the Han River is not only a vital grain production region and economic center, but also a source of the middle route of the South-to-North Water Transfer Project (SNWTP).

The study area, Shiquan catchment, is a sub-basin situated in the upper Han River basin, spanning an area of 23,805 km^2 and with an altitudinal range of 357–3,549 (Figure 2). The catchment receives an annual precipitation amount of approximately 800 mm, belonging to the humid area in China. The rainfall distribution is quite uneven over a year in that precipitation in summer accounts for over 70%.

The presented models were applied to daily streamflow simulation in Shiquan catchment. In this paper, the daily precipitation, evapotranspiration, and streamflow observations from 2004 to 2014 were collected from the China Hydrological Yearbook. There were no missing values in the data series.

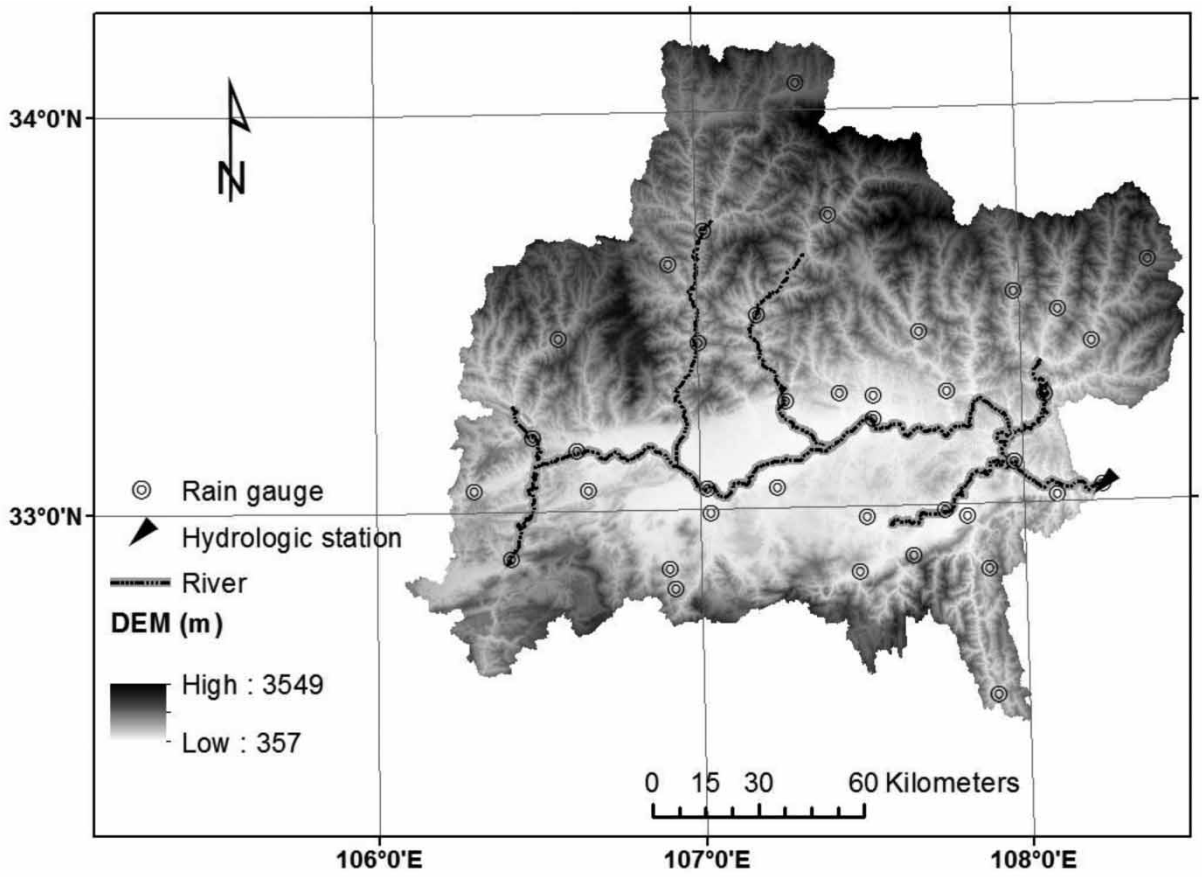

Figure 2 | A map of Shiquan catchment.

RESULTS AND DISCUSSION

XAJ model simulation

The daily observations from 2004 to 2014 were split into two subseries: the data from 2004 to 2012 were used to calibrate the parameters in the XAJ model, while the remaining two years' data were used for model validation. In this paper, the multi-objective optimization technique was employed to find the optimal values of the associated parameters. First, the measures of NSE, RMSE, PBIAS, MAE, and R were taken into consideration. Then, these measures were assigned with equal weights and converted to a comprehensive measure for parameter optimization. The optimized parameters of the XAJ model are shown in Table 2 and the comparison of observation and simulation are displayed in Figure 3. As the figure depicts, the observed daily streamflow and simulated values from the XAJ model exhibited good fitness. The measure values of NSE, RMSE, PBIAS, MAE, and R under optimized parameters during calibration were 0.85, 239 m^3/s, 1.74%, 113 m^3/s, and 0.92, respectively, while those values during validation were 0.80, 254 m^3/s, −8.34%, 133 m^3/s, and 0.92, respectively. Overall, the calibration and validation results of the XAJ model applied to Shiquan station were good. Thus, the corresponding parameters and simulation results were applicable in this study.

Predictor identification

Two types of data, accumulated precipitation and antecedent streamflow, are commonly used in data-driven models for daily streamflow modeling. In this paper, accumulated precipitation and antecedent streamflow of the

Table 2 | List of parameters of XAJ model and its calibration results

Sub-model	Parameter	Description	Value
Evapotranspiration	*KC*	Ratio of potential evapotranspiration to pan evaporation	1.030
	UM	Tension water capacity of upper layer	10.012
	LM	Tension water capacity of lower layer	66.777
	C	Coefficient of deep evapotranspiration	0.157
Runoff production	*WM*	Areal mean tension water capacity	169.739
	B	Exponent of the tension water capacity curve	0.400
	IM	Ratio of the impervious to the total area of the basin	0.010
Runoff separation	*SM*	Free water capacity	19.999
	EX	Exponent of the freewater capacity curve	1.250
	KG	Outflow coefficient of the freewater storage to groundwater	0.284
	KI	Outflow coefficient of the freewater storage to interflow	0.416
Runoff concentration	*CI*	Recession constant of inflow storage	0.848
	CG	Recession constant of groundwater storage	0.996
	CS	Recession constant in the lag-and-route method	0.232

past 1 day, 2 days, 3 days, and 4 days ($\sum_{t-1}^{t} p_t$, $\sum_{t-2}^{t} p_t$, $\sum_{t-3}^{t} p_t$, $\sum_{t-4}^{t} p_t$, Q_{t-1}, Q_{t-2}, Q_{t-3}, Q_{t-4}) were used as possible factors. The correlation coefficient, autocorrelation function (ACF), and partial autocorrelation function (PACF) were adopted to choose the most relevant factors for streamflow simulation (Özger *et al.* 2020). The results are shown in Table 3 and Figure 4.

It can be concluded from Table 3 that the accumulated precipitation of past 2 days $\sum_{t-2}^{t} p_t$ and the antecedent streamflow of past 1 day Q_{t-1} had a correlation coefficient over 0.7. Moreover, the relevant antecedent streamflow can be identified by ACF. As shown in Figure 4, the ACF values were high until lag-3, and the partial autocorrelation function (PACF) was truncated at lag-3. It is indicated that the current daily streamflow has a relatively stronger relationship with the previous three daily streamflows. Thus, the models were established with one lag time value at first, then one and two lag times were used, and finally one, two, and three lag times were used as inputs (Table 4). The performance statistics of different input variables for RF models are presented in Table 5. It is observed that model 7 yielded the highest NSE (0.889) and R (0.945) and lowest RMSE (204 m^3/s) and MAE (71 m^3/s) among these RF models. Meanwhile, its PBIAS value was also very low (0.149%). As well, model 1 performed better than models 2, 3, and 5 on all evaluation statistics, indicating that Q_{t-1} was very important in the prediction of Q_t. The performance of models 1, 4, and 6 had a similar level of accuracy, while model 7 outperformed them all. Ultimately, model 7 outperformed models 1–6, thus $\sum_{t-2}^{t} p_t$, Q_{t-1}, Q_{t-2}, Q_{t-3} were used for streamflow simulation in this paper.

Analysis of modeling results

The wavelet decomposition method was introduced to improve the accuracy of the developed model. First, the relevant factors such as accumulated precipitation, antecedent streamflow, and simulated streamflow from the XAJ model, were transformed to approximate component and detail components under the decomposition level. Therefore, the number of input variables increased from 4 to 20 in the hybrid models (WRF and XAJ-WRF models). Quantitative results of the XAJ model, RF model, and hybrid models are presented in Table 6. In fact, a wide range of mother wavelets employed on the time series can provide various results. Therefore, 14 wavelet functions, which originated from five various wavelet families with different orders of subclass, were investigated. The performance statistics of WRF and XAJ-WRF models were the average value of the 14 cases with different wavelet functions.

Table 6 indicates that the XAJ-RF model had a relatively higher level of accuracy (NSE = 0.916, RMSE = 177 m^3/s, and MAE = 66 m^3/s) than that of the XAJ model (NSE = 0.843, RMSE = 242 m^3/s, and MAE = 117 m^3/s) and RF model (NSE = 0.889, RMSE = 204 m^3/s, and MAE = 71 m^3/s) in most performance statistics. However, the

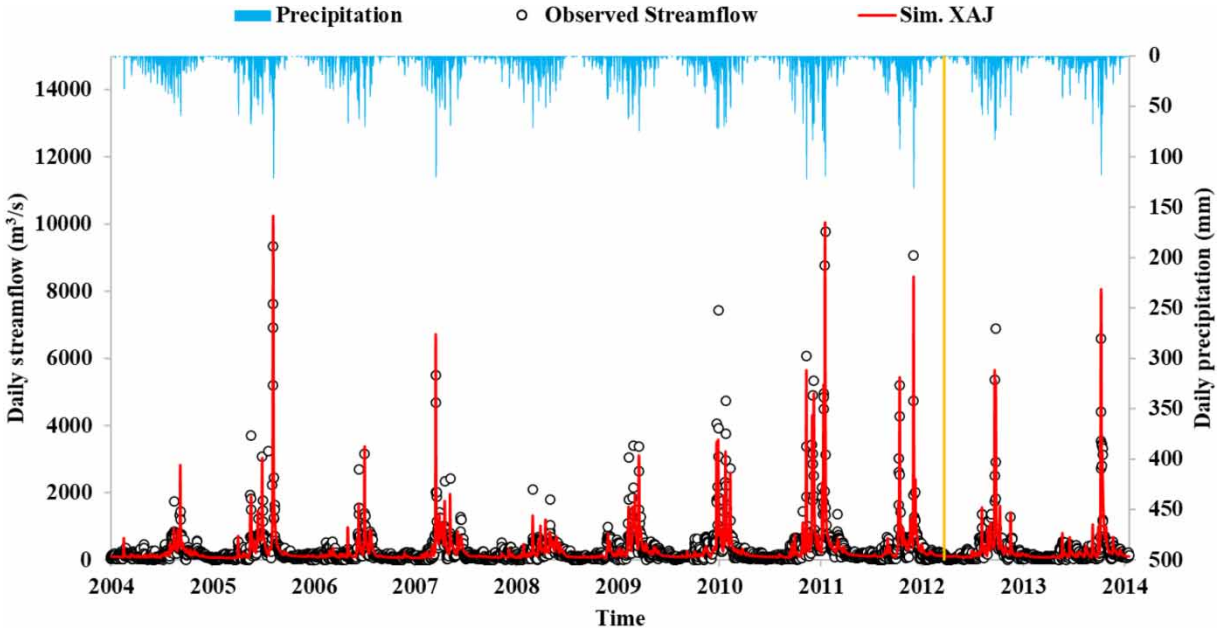

Figure 3 | Comparison of observed and simulated daily streamflow to Shiquan station during calibration and validation period.

Table 3 | The correlation coefficient between possible predictors and observed daily streamflow

	$\sum_{t-1}^{t} p_t$	$\sum_{t-2}^{t} p_t$	$\sum_{t-3}^{t} p_t$	$\sum_{t-4}^{t} p_t$	Q_{t-1}	Q_{t-2}	Q_{t-3}	Q_{t-4}	Q_t
$\sum_{t-1}^{t} p_t$	1								
$\sum_{t-2}^{t} p_t$	0.920	1							
$\sum_{t-3}^{t} p_t$	0.823	0.945	1						
$\sum_{t-4}^{t} p_t$	0.755	0.873	0.960	1					
Q_{t-1}	0.478	0.625	0.671	0.682	1				
Q_{t-2}	0.261	0.428	0.569	0.623	0.764	1			
Q_{t-3}	0.179	0.256	0.400	0.529	0.543	0.764	1		
Q_{t-4}	0.170	0.198	0.262	0.386	0.440	0.543	0.764	1	
$\boldsymbol{Q_t}$	0.676	0.700	0.699	0.696	0.764	0.543	0.440	0.404	1

Q_t represents the observed daily streamflow at t.

PBIAS of the XAJ-RF model was slightly larger than those of the XAJ model and RF model. Moreover, compared to the RF and XAJ-RF models, the NSE values of WRF and XAJ-WRF were raised from 0.889 to 0.942 and from 0.916 to 0.947, respectively. Other performance statistics, such as MAE and R, also showed slight improvements. The MAE of the XAJ model was decreased to 43 and 62% by the XAJ-RF model and XAJ-WRF model, respectively. The PBIAS of the wavelet-based models (WRF and XAJ-WRF) was within the range of ±6%. Concerning $F_{0.05,6,49}$, F_0 values obtained by the five models have accepted the hypothesis and indicated accurate estimation of daily streamflow modeling. Overall, these statistics indicate that the application of wavelet analysis contributed to the increasing accuracy of hydrological modeling.

The scatter plots between observed daily streamflow and simulated daily streamflow are displayed in Figure 5. It can be observed that the XAJ-WRF model showed good agreement of observations and simulations among all proposed models, particularly in medium streamflow, but it seems

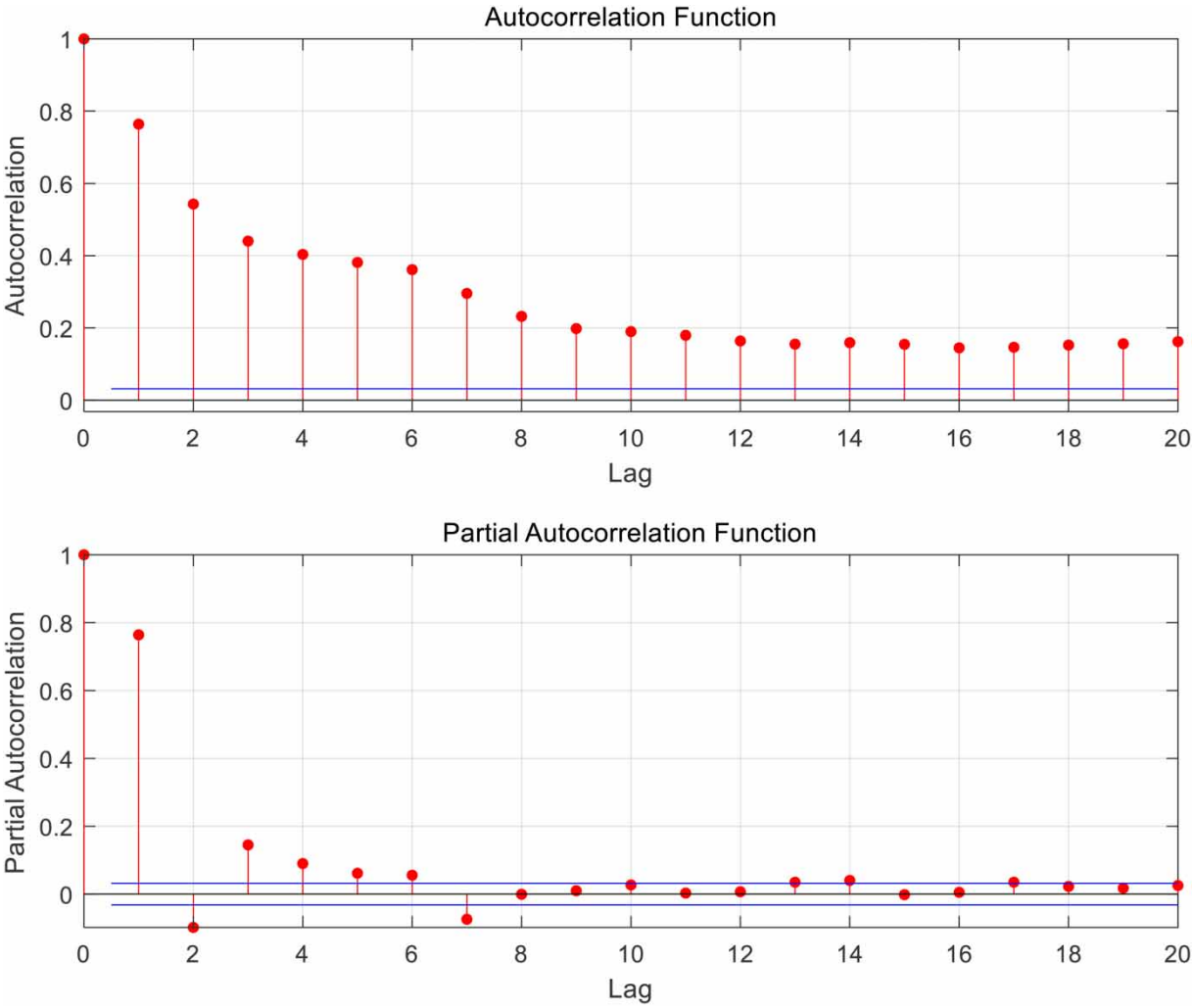

Figure 4 | Autocorrelation and partial autocorrelation graphs of observed daily streamflow for Shiquan station.

Table 4 | Input variables for RF model

Considered time lags	Model number	Input variables	Output variable
One time lag	Model 1	$\sum_{t-2}^{t} p_t, Q_{t-1}$	Q_t
	Model 2	$\sum_{t-2}^{t} p_t, Q_{t-2}$	Q_t
	Model 3	$\sum_{t-2}^{t} p_t, Q_{t-3}$	Q_t
Two time lags	Model 4	$\sum_{t-2}^{t} p_t, Q_{t-1}, Q_{t-2}$	Q_t
	Model 5	$\sum_{t-2}^{t} p_t, Q_{t-2}, Q_{t-3}$	Q_t
	Model 6	$\sum_{t-2}^{t} p_t, Q_{t-1}, Q_{t-3}$	Q_t
Three time lags	Model 7	$\sum_{t-2}^{t} p_t, Q_{t-1}, Q_{t-2}, Q_{t-3}$	Q_t

there was no significant improvement in high streamflow simulation over 8,000 m^3/s. The possible reason lies in the fact that the RF model always provided final results by averaging all trees for regression tasks. Therefore, the performance of the RF method on simulating extreme values is not so good. As well, compared to the other models, the scatters of observed daily streamflow with simulated values from XAJ-WRF and WRF models were distributed symmetrically and more concentrated on both sides of the 1:1 line.

Figures 6 and 7 present the NSE, RMSE, and R values of XAJ, RF, XAJ-RF, WRF, and XAJ-WRF models in yearly scales. It was observed from Figure 6 that the XAJ-WRF model yielded the highest level of NSE values, with ten years NSEs exceeding 0.9. The NSEs of WRF and XAJ-RF model were slightly lower than those of the XAJ-WRF model, with nine and seven years NSEs exceeding 0.9.

Table 5 | The performance statistics of different input variables for RF model

Models	Model 1	Model 2	Model 3	Model 4	Model 5	Model 6	Model 7
Statistics							
NSE	0.858	0.852	0.839	0.860	0.835	0.858	0.889
RMSE	230 m^3/s	235 m^3/s	245 m^3/s	229 m^3/s	249 m^3/s	230 m^3/s	204 m^3/s
PBIAS	0.093%	− 0.477%	− 0.699%	− 0.190%	0.162%	− 0.467%	0.149%
MAE	81 m^3/s	95 m^3/s	103 m^3/s	79 m^3/s	93 m^3/s	80 m^3/s	71 m^3/s
R	0.928	0.924	0.917	0.930	0.921	0.928	0.945

Table 6 | The simulation statistics of XAJ, RF, XAJ-RF, WRF and XAJ-WRF models

Models	NSE	RMSE	PBIAS	MAE	R	F_0
XAJ	0.843	242 m^3/s	0.058%	117 m^3/s	0.921	1.315
RF	0.889	204 m^3/s	0.149%	71 m^3/s	0.945	1.178
XAJ-RF	0.916	177 m^3/s	− 0.907%	66 m^3/s	0.958	0.802
WRF	0.942	148 m^3/s	0.531%	44 m^3/s	0.975	0.613
XAJ-WRF	0.947	141 m^3/s	0.579%	44 m^3/s	0.976	0.647

In most years, the RF model has higher NSEs than the XAJ model. As depicted in Figure 7, the XAJ model and RF model achieved higher RMSEs than hybrid models in most of the period except 2004, 2009, and 2014. Thus, hybrid models demonstrated better performance in this regard. In contrast to the XAJ-RF model, the yearly RMSE values increased 35% in the XAJ-WRF model on average. In conclusion, these results indicate that the XAJ-RF model worked better than the other benchmark models (XAJ and RF) and the introduction of wavelet transform technique can effectively enhance the level of modeling accuracy. The reasons may lie in the fact that wavelet analysis can reveal the temporal variation of the rainfall-runoff relationship and capture the small but meaningful characteristics in the datasets.

Comparison of various wavelet functions

To investigate the impact of various wavelet functions on WRF and XAJ-WRF model, 14 wavelet functions which originated from five various wavelet families with different orders of subclass were employed. The simulation results are listed in Table 7.

As seen in Table 7, the XAJ-WRF model developed by sym2 wavelet function had the best efficiency (NSE = 0.951, RMSE = 135 m^3/s, and R = 0.978). Compared to the XAJ-RF model, its corresponding increases in NSE and R values were 0.035 and 0.02, respectively, whereas RMSE and MAE values decreased 42 m^3/s and 24 m^3/s, respectively. The XAJ-WRF model using dmey wavelet function stood as the worst performance among 14 mother wavelets (NSE = 0.937, RMSE = 153 m^3/s, and R = 0.971), but it was still better than that of the XAJ-RF model. The NSE, PBIAS, and R of the XAJ-RF model were raised from 0.916 to 0.937, −0.907% to 0.362%, and 0.958 to 0.971, respectively. Meanwhile, the RMSE and MAE dropped by 14 and 16%, respectively. As a whole, the impact of various mother wavelets on the XAJ-WRF model was limited in this research. As shown in Table 8, the interval of variation of RMSE, MAE, and R values was small. The changing intervals of NSE and PBIAS values were relatively larger. The NSE and PBIAS values of the WRF model varied from 0.934 to 0.946 and 0.315% to 0.793%, whereas those of XAJ-WRF varied from 0.937 to 0.951 and 0.362% to 0.753%, respectively. Overall, the XAJ-

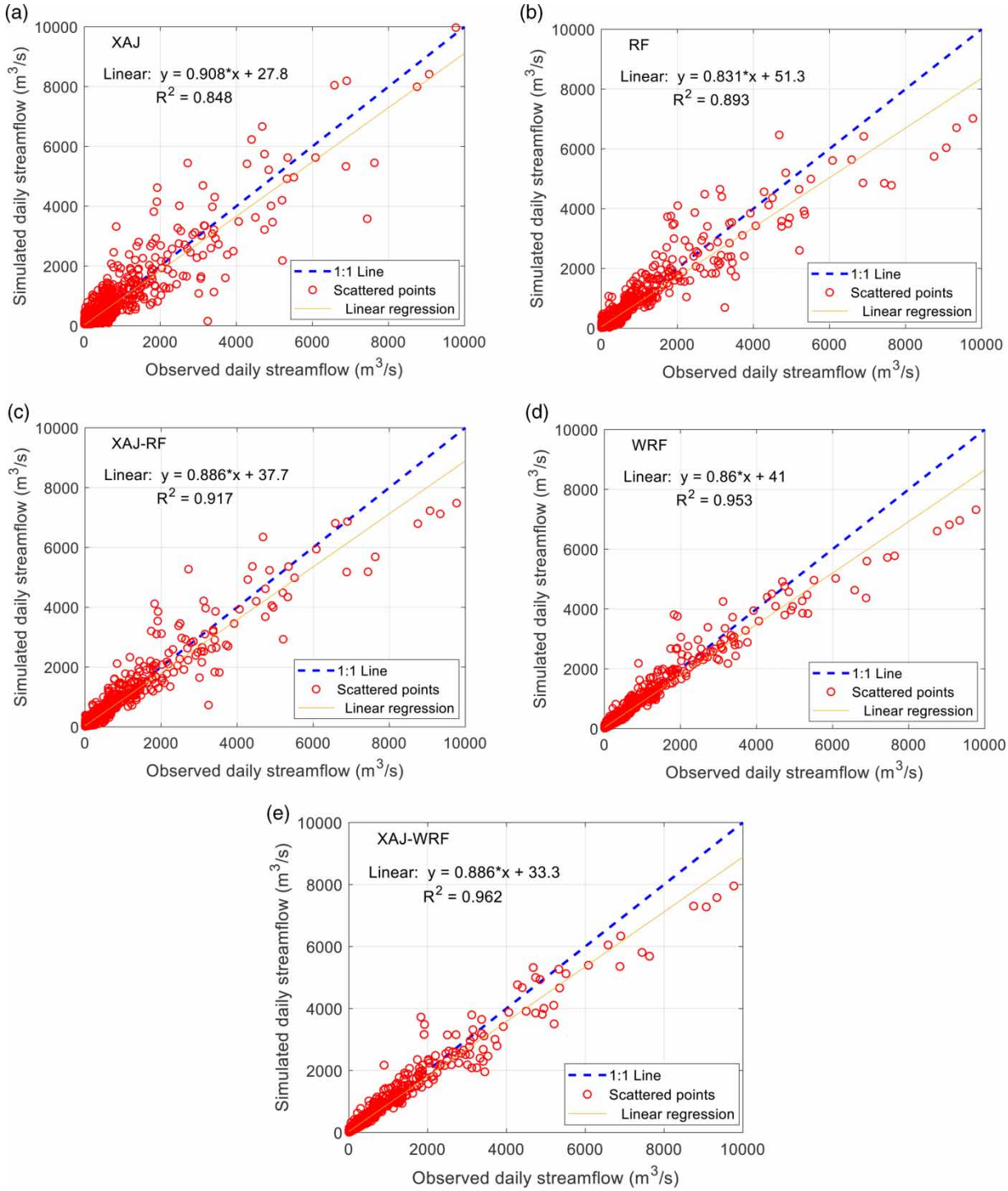

Figure 5 | Scatterplots of observed and simulated daily streamflow XAJ, RF, XAJ-RF, WRF, and XAJ-WRF models.

WRF model worked better than XAJ-RF and WRF models. Moreover, the proposed model can be applied to daily streamflow prediction once the future precipitation during the lead time can be obtained. The XAJ-RF model can run for operational streamflow forecasting.

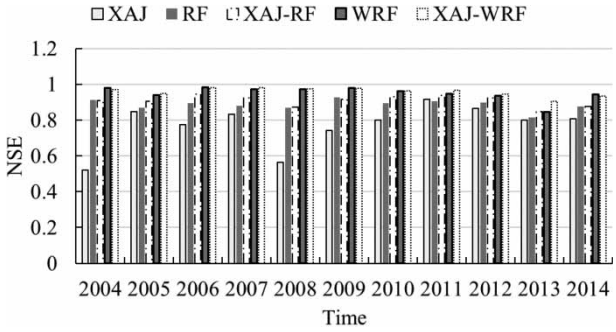

Figure 6 | Comparison of NSE values of XAJ, RF, XAJ-RF, WRF, and XAJ-WRF models.

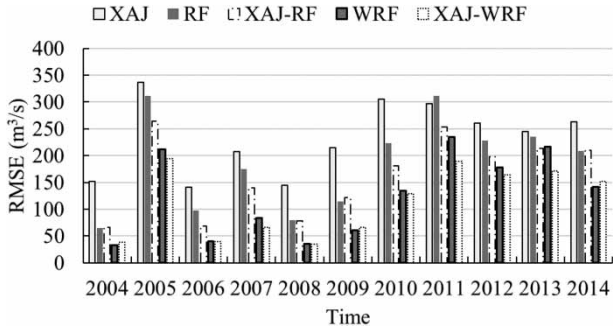

Figure 7 | Comparison of RMSE values of XAJ, RF, XAJ-RF, WRF, and XAJ-WRF models.

CONCLUSIONS

This paper compared the performance of the XAJ model and RF method in daily streamflow simulation, and proposed several hybrid models based on XAJ model, wavelet analysis, and RF method. In this study, five models were developed for daily streamflow modeling: (1) Xinanjiang model (XAJ); (2) random forests model (RF) with the inputs of accumulated precipitation and antecedent streamflow; (3) hybrid model (XAJ-RF), with the inputs of antecedent streamflow and simulated streamflow from the XAJ model; (4) wavelet-based RF model (WRF) using subseries of accumulated precipitation and antecedent streamflow as input variables; and (5) hybrid XAJ-WRF model using subseries of antecedent streamflow and simulated streamflow from the XAJ model as input variables. The first two were established as benchmark models for the third hybrid model, while the last two models adopted wavelet transformation technique to further improve the level of accuracy. The proposed methods were applied to Shiquan station, located in the Upper Han River basin in China. Based on the results of the case study, the following conclusions were drawn.

1. The case study indicated that the XAJ-RF model had a relatively higher level of accuracy (NSE = 0.916, RMSE

Table 7 | The simulation statistics of WRF and XAJ-WRF models with various mother wavelets

	WRF model						XAJ-WRF model					
Wavelet function	**NSE**	**RMSE**	**PBIAS**	**MAE**	**R**	F_0	**NSE**	**RMSE**	**PBIAS**	**MAE**	**R**	F_0
haar	0.941	148 m^3/s	0.333%	42 m^3/s	0.973	0.594	0.948	140 m^3/s	0.577%	42 m^3/s	0.976	0.517
db1	0.946	142 m^3/s	0.529%	41 m^3/s	0.976	0.552	0.949	138 m^3/s	0.644%	41 m^3/s	0.977	0.499
db2	0.941	148 m^3/s	0.327%	42 m^3/s	0.974	0.610	0.950	137 m^3/s	0.504%	42 m^3/s	0.977	0.500
db3	0.942	147 m^3/s	0.383%	43 m^3/s	0.975	0.602	0.948	140 m^3/s	0.588%	43 m^3/s	0.977	0.527
db4	0.941	148 m^3/s	0.607%	44 m^3/s	0.975	0.621	0.946	142 m^3/s	0.426%	44 m^3/s	0.976	0.543
coif1	0.944	145 m^3/s	0.739%	42 m^3/s	0.976	0.594	0.950	136 m^3/s	0.731%	42 m^3/s	0.978	0.504
coif2	0.941	148 m^3/s	0.492%	43 m^3/s	0.974	0.612	0.950	137 m^3/s	0.500%	44 m^3/s	0.977	0.505
coif3	0.939	150 m^3/s	0.793%	45 m^3/s	0.975	0.650	0.945	143 m^3/s	0.622%	45 m^3/s	0.976	0.565
coif4	0.942	147 m^3/s	0.315%	46 m^3/s	0.975	0.600	0.940	150 m^3/s	0.605%	47 m^3/s	0.973	0.621
sym2	0.941	148 m^3/s	0.556%	42 m^3/s	0.975	0.619	0.951	135 m^3/s	0.622%	42 m^3/s	0.978	0.489
sym3	0.942	147 m^3/s	0.703%	42 m^3/s	0.976	0.618	0.948	139 m^3/s	0.674%	43 m^3/s	0.977	0.530
sym4	0.943	146 m^3/s	0.590%	43 m^3/s	0.976	0.602	0.945	143 m^3/s	0.753%	44 m^3/s	0.976	0.565
sym5	0.942	147 m^3/s	0.437%	44 m^3/s	0.975	0.603	0.948	139 m^3/s	0.499%	45 m^3/s	0.977	0.519
dmey	0.934	158 m^3/s	0.635%	50 m^3/s	0.971	0.706	0.937	153 m^3/s	0.362%	51 m^3/s	0.971	0.647

Table 8 | The maximum and minimum statistics of WRF and XAJ-WRF models with various mother wavelets

	WRF model		XAJ-WRF model	
Performance statistics	**Max**	**Min**	**Max**	**Min**
NSE	0.946	0.934	0.951	0.937
RMSE	158 m^3/s	142 m^3/s	153 m^3/s	135 m^3/s
PBIAS	0.793%	0.315%	0.753%	0.362%
MAE	50 m^3/s	41 m^3/s	51 m^3/s	41 m^3/s
R	0.976	0.971	0.978	0.971

$= 177\ m^3/s$, and MAE $= 66\ m^3/s$) than that of the XAJ model (NSE $= 0.843$, RMSE $= 242\ m^3/s$, and MAE $= 117\ m^3/s$) and RF model (NSE $= 0.889$, RMSE $= 204\ m^3/s$, and MAE $= 71\ m^3/s$). These results indicated that the coupled XAJ-RF model can be effectively applied, providing a useful alternative for daily streamflow simulation.

2. To investigate the impact of various mother wavelets, 14 wavelet functions from Haar, Daubechies, Coiflets, Symlets and DMeyer families were tested, and acted as preprocessors to the input variables of the RF model. In contrast to the XAJ-RF model, the yearly RMSE values increased 35% by XAJ-WRF model on average. The XAJ-WRF model developed by sym2 wavelet function had the best efficiency (NSE $= 0.951$, RMSE $= 135\ m^3/s$, and R $= 0.978$). Moreover, even for the worst XAJ-WRF model with dmey wavelet function, the NSE, PBIAS, and R of the XAJ-RF model were raised from 0.916 to 0.937, −0.907% to 0.362%, and 0.958 to 0.971, respectively. Therefore, the introduction of wavelet analysis made contributions to the increased accuracy.

With the introduction of numerical weather prediction or precipitation forecasting, the proposed method can be used for daily streamflow prediction with different lead times. It can also be applied for operational forecasting.

ACKNOWLEDGEMENTS

This work was supported by the Special Foundation for National Program on Key Basic Research Project (2016|YFC0402703, 2019|YFC0409005, 2019YFC0409003), The Fundamental Research Funds for the Central Universities (B200201027), National Natural Science Foundation of China (51709077) and Open Research Fund of the Yellow River Sediment Key Laboratory of Ministry of Water Resources (201804).

DATA AVAILABILITY STATEMENT

All relevant data are included in the paper or its Supplementary Information.

REFERENCES

Ahirwar, A., Jain, M. K. & Perumal, M. 2018 Performance of the Xinanjiang model. *Hydrologic Modeling* **18**, 715–731.

Babovic, V. 2005 Data mining in hydrology. *Hydrological Processes* **197**, 1511–1515.

Babovic, V. 2009 Introducing knowledge into learning based on genetic programming. *Journal of Hydroinformatics* **11** (3–4), 181–193.

Babovic, V., Cañizares, R., Jensen, H. R. & Klinting, A. 2001 Neural networks as routine for error updating of numerical models. *Journal of Hydraulic Engineering* **1273**, 181–193.

Bai, P., Liu, X., Liang, K., Liu, X. & Liu, C. 2016 A comparison of simple and complex versions of the Xinanjiang hydrological model in predicting runoff in ungauged basins. *Hydrology Research* **485**, 1282–1295.

Brath, A., Montanari, A. & Toth, E. 2002 Neural networks and non-parametric methods for improving real-time flood forecasting through conceptual hydrological models. *Hydrology and Earth System Sciences* **6**, 627–639.

Breiman, L. 2001 Random forests. *Machine Learning* **45** (1), 5–32.

Chadalawada, J. & Babovic, V. 2019 Review and comparison of performance indices for automatic model induction. *Journal of Hydroinformatics* **21** (1), 13–31.

Chadalawada, J., Havlicek, V. & Babovic, V. 2017 A genetic programming approach to system identification of rainfall-runoff models. *Water Resources Management* **31**, 3975–3992.

Chadalawada, J., Herath, H. M. V. V. & Babovic, V. 2020 Hydrologically informed machine learning for rainfall–runoff modeling: a genetic programming-based toolkit for automatic model induction. *Water Resources Research* **56** (4), e2019WR026933.

Cheng, C.-T., Zhao, M.-Y. & Wu, X.-Y. 2006 Using genetic algorithm and TOPSIS for Xinanjiang model calibration with a single procedure. *Journal of Hydrology* **316**, 129–140.

Chou, C.-m. 2013 Enhanced accuracy of rainfall–runoff modeling with wavelet transform. *Journal of Hydroinformatics* **15**, 392–404.

Corzo, P. G. A. & Solomatine, D. 2014 Comparative analysis of conceptual models with error correction, artificial neural networks and committee models. In: *EGU General Assembly Conference Abstracts*.

Feyen, L., Vázquez, R., Christiaens, K., Sels, O. & Feyen, J. 2000 Application of a distributed physically-based hydrological model to a medium size catchment. *Hydrology and Earth System Sciences* **4** (1), 47–63.

Gan, T. Y. & Biftu, G. 1996 Automatic calibration of conceptual rainfall-runoff models: optimization algorithms, catchment conditions, and model structure. *Water Resources Research* **32**, 3513–3524.

Ghaith, M., Siam, A., Li, Z. & El-Dakhakhni, W. 2020 Hybrid hydrological data-driven approach for daily streamflow forecasting. *Journal of Hydrologic Engineering* **25**, 04019063.

Homaei, F. & Najafzadeh, M. 2020 A reliability-based probabilistic evaluation of the wave-induced scour depth around marine structure piles. *Ocean Engineering* **196**, 106818.1–106818.12.

Humphrey, G. B., Gibbs, M. S., Dandy, G. C. & Maier, H. R. 2016 A hybrid approach to monthly streamflow forecasting: integrating hydrological model outputs into a Bayesian artificial neural network. *Journal of Hydrology* **540**, 623–640.

Jayawardena, A. & Zhou, M. 2000 A modified spatial soil moisture storage capacity distribution curve for the Xinanjiang model. *Journal of Hydrology* **227**, 93–113.

Jiang, T., Chen, Y., Xu, C., Chen, X., Chen, X. & Singh, V. P. 2007 Comparison of hydrological impacts of climate change simulated by six hydrological models in the Dongjiang Basin, South China. *Journal of Hydrology* **336**, 316–333.

Karpatne, A., Atluri, G., Faghmous, J. H., Steinbach, M., Banerjee, A., Ganguly, A., Shekhar, S., Samatova, N. & Kumar, V. 2017 Theory-guided data science: a new paradigm for scientific discovery from data. *IEEE Transactions on Knowledge and Data Engineering* **29** (10), 2318–2331.

Kavetski, D., Kuczera, G. & Franks, S. 2006 Calibration of conceptual hydrological models revisited: 1. Overcoming numerical artefacts. *Journal of Hydrology* **320**, 173–186.

Kisi, O. & Shiri, J. 2011 Precipitation forecasting using wavelet-genetic programming and wavelet-neuro-fuzzy conjunction models. *Water Resources Management* **25**, 3135–3152.

Li, H., Zhang, Y., Chiew, F. H. S. & Xu, S. 2009 Predicting runoff in ungauged catchments by using xinanjiang model with MODIS leaf area index. *Journal of Hydrology* **370** (1–4), 155–162.

Li, B., Yang, G., Wan, R., Dai, X. & Zhang, Y. 2016 Comparison of random forests and other statistical methods for the prediction of lake water level: a case study of the Poyang Lake in China. *Hydrology Research* **47** (S1), 69–83.

Li, X., Sha, J. & Wang, Z. L. 2019 Comparison of daily streamflow forecasts using extreme learning machines and the random forest method. *Hydrological Sciences Journal* **64** (15), 1857–1866.

Liang, Z., Tang, T., Li, B., Liu, T. & Hu, Y. 2017 Long-term streamflow forecasting using SWAT through the integration of the random forests precipitation generator: case study of Danjiangkou reservoir. *Hydrology Research* **49** (5), nh2017085.

Liang, Z., Xiao, Z., Wang, J., Sun, L. & Wu, Y. 2019 An improved chaos similarity model for hydrological forecasting. *Journal of Hydrology* **577**, 123953.

Liong, S. Y., Gautam, T. R., Khu, S. T., Babovic, V., Keijzer, M. & Muttil, N. 2002 Genetic programming: a new paradigm in rainfall runoff modeling. *Journal of the American Water Resources Association* **383**, 705–718.

Mehrparvar, M. & Asghari, K. 2018 Modular optimized data assimilation and support vector machine for hydrologic modeling. *Journal of Hydroinformatics* **20** (3), 728–738.

Meng, C., Zhou, J., Zhong, D., Wang, C. & Guo, J. 2018 An improved grid-Xinanjiang model and its application in the Jinshajiang Basin, China. *Water* **10**, 1265.

Meshgi, A., Schmitter, P., Chui, T. & Babovic, V. 2015 Development of a modular streamflow model to quantify runoff contributions from different land uses in tropical urban environments using genetic programming. *Journal of Hydrology* **525**, 711–723.

Moriasi, D. N., Arnold, J. G., Liew, M. W. V., Bingner, R. L., Harmel, R. D. & Veith, T. L. 2007 Model evaluation guidelines for systematic quantification of accuracy in watershed simulations. *Transactions of the ASABE* **50** (3), 885–900.

Muñoz, P., Orellana-Alvear, J., Willems, P. & Célleri, R. 2018 Flash-flood forecasting in an Andean mountain catchment – development of a step-wise methodology based on the random forest algorithm. *Water* **10**, 1519.

Najafzadeh, M. & Ghaemi, A. 2019 Prediction of the five-day biochemical oxygen demand and chemical oxygen demand in natural streams using machine learning methods. *Environmental Monitoring and Assessment* **191** (6), 380.

Najafzadeh, M. & Kargar, A. R. 2019 Gene-expression programming, evolutionary polynomial regression, and model tree to evaluate local scour depth at culvert outlets. *Journal of Pipeline Systems Engineering and Practice* **103**, 04019013.1–04019013.12.

Najafzadeh, M. & Oliveto, G. 2020 Riprap incipient motion for overtopping flows with machine learning models. *Journal of Hydroinformatics* **22** (4), 749–767.

Najafzadeh, M. & Zeinolabedini, M. 2018 Derivation of optimal equations for prediction of sewage sludge quantity using wavelet conjunction models: an environmental assessment. *Environmental Science and Pollution Research* **25**, 22931–22943.

Napolitano, G., See, L. & Savi, F. 2009 Integrating neural networks and conceptual modelling for flood forecasting on the Tiber River. Egu General Assembly Conference. In: *EGU General Assembly Conference Abstracts*.

Nghi, V. V., Lam, D. T. & Dung, D. D. 2008 Comparison of two hydrological model simulations using Nam and Xinanjiang for Nong Son catchment. *Vietnam Journal of Mechanics* **30** (1), 43–54.

Noori, N. & Kalin, L. 2016 Coupling SWAT and ANN models for enhanced daily streamflow prediction. *Journal of Hydrology* **53** (3), 141–151.

Nourani, V. & Parhizkar, M. 2013 Conjunction of SOM-based feature extraction method and hybrid wavelet-ANN approach for rainfall-runoff modeling. *Journal of Hydroinformatics* **15** (3), 829–848.

Özger, M., Başakın, E. E., Ekmekcioğlu, Ö. & Hacısüleyman, V. 2020 Comparison of wavelet and empirical mode decomposition hybrid models in drought prediction. *Computers and Electronics in Agriculture* **179**, 105851. doi:10.1016/j.compag.2020.105851.

Papacharalampous, G. A. & Tyralis, H. 2018 Evaluation of random forests and prophet for daily streamflow forecasting. *Advances in Geosciences* **45**, 201–208.

Rahman, M. & Lu, M. 2015 Model spin-up behavior for wet and dry basins: a case study using the Xinanjiang model. *Water* **7**, 4256–4273.

Rathinasamy, M., Khosa, R., Adamowski, J., Ch, S., Partheepan, G., Anand, J. & Narsimlu, B. 2015 Wavelet-based multiscale performance analysis: an approach to assess and improve hydrological models. *Water Resources Research* **50** (12), 9721–9737.

Raza, A., Shoaib, M., Faiz, M. A., Baig, F. & Zubair, M. 2020 Comparative assessment of reference evapotranspiration estimation using conventional method and machine learning algorithms in four climatic regions. *Pure and Applied Geophysics* **177**, 4479–4508.

Ren, W. W., Yang, T., Huang, C. S., Xu, C. Y. & Shao, Q. X. 2018 Improving monthly streamflow prediction in alpine regions: integrating HBV model with Bayesian neural network. *Stochastic Environmental Research & Risk Assessment* **32** (12), 1–16.

Rezaie-Balf, M., Zahmatkesh, Z. & Kim, S. 2017 Soft computing techniques for rainfall-runoff simulation: local non–parametric paradigm vs. model classification methods. *Water Resources Management* **31** (12), 3843–3865.

Sadeghi, G., Najafzadeh, M. & Ameri, M. 2019 Thermal characteristics of evacuated tube solar collectors with coil inside: an experimental study and evolutionary algorithms. *Renewable Energy* **151**, 575–588.

Schnier, S. & Cai, X. 2014 Prediction of regional streamflow frequency using model tree ensembles. *Journal of Hydrology* **517** (5), 298–309.

Solomatine, D. & Ostfeld, A. 2008 Data-driven modelling: some past experiences and new approaches. *Journal of Hydroinformatics* **10** (1), 3–22.

Sun, Y., Babovic, V. & Chan, E. S. 2010 Multi-step-ahead model error prediction using time-delay neural networks combined with chaos theory. *Journal of Hydrology* **395** (1–2), 109–116.

Tian, F., Hu, H., Sun, Y., Li, H. & Lu, H. 2019 Searching for an optimized single-objective function matching multiple objectives with automatic calibration of hydrological models. *Chinese Geographical Science* **29**, 934–948.

Wang, Z., Lai, C., Chen, X., Yang, B., Zhao, S. & Bai, X. 2015 Flood hazard risk assessment model based on random forest. *Journal of Hydrology* **527**, 1130–1141.

Xu, T. & Valocchi, A. J. 2015 Data-driven methods to improve baseflow prediction of a regional groundwater model. *Computers & Geosciences* **85**, 124–136.

Xu, D., Wang, W., Chau, K., Cheng, C. & Chen, S. 2013 Comparison of three global optimization algorithms for calibration of the Xinanjiang model parameters. *Journal of Hydroinformatics* **151**, 174–193.

Yao, C., Li, Z., Yu, Z. & Zhang, K. 2012 A priori parameter estimates for a distributed, grid-based Xinanjiang model using geographically based information. *Journal of Hydrology* **468–469**, 47–62. doi:10.1016/j.jhydrol.2012.08.025.

Yao, C., Zhang, K., Yu, Z., Li, Z. & Li, Q. 2014 Improving the flood prediction capability of the Xinanjiang model in ungauged nested catchments by coupling it with the geomorphologic instantaneous unit hydrograph. *Journal of Hydrology* **517**, 1035–1048.

Yu, X., Liong, S. Y. & Babovic, V. 2004 EC-SVM approach for real-time hydrologic forecasting. *Journal of Hydroinformatics* **63**, 209–223.

Yuan, F., Tung, Y. K. & Ren, L. 2016 Projection of future streamflow changes of the Pearl River basin in China using two delta-change methods. *Hydrology Research* **47** (1), 217–238.

Zeinolabedini, M. & Najafzadeh, M. 2019 Comparative study of different wavelet-based neural network models to predict sewage sludge quantity in wastewater treatment plant. *Environmental Monitoring and Assessment* **191**, 163.

Zhang, Z., Zhang, Q., Singh, V. P. & Shi, P. 2018 River flow modelling: comparison of performance and evaluation of uncertainty using data-driven models and conceptual hydrological model. *Stochastic Environmental Research and Risk Assessment* **32**, 2667–2682.

Zhao, R. 1977 *Flood Forecasting Method for Humid Regions of China*. East China College of Hydraulic Engineering, Nanjing, China, pp. 19–51, 135–170, 206–224 (in Chinese).

Zhao, R. 1992 The Xinanjiang model applied in China. *Journal of Hydrology* **135**, 371–378.

Zhao, R., Zhang, Y., Fang, L., Liu, X. & Zhang, Q. 1980 The Xinanjiang model. Proceedings of the Oxford Symposium. *IAHS Publication* **129**, 351–356.

Zhu, J. & Pierskalla, W. 2016 Applying a weighted random forests method to extract karst sinkholes from LiDAR data. *Journal of Hydrology* **533**, 343–352.

Zoran, V., Vojislav, K. & Vladan, B. 2003 Hybrid approach for modeling wet weather response in wastewater systems. *Journal of Water Resources Planning and Management* **129** (6), 511–521.

First received 2 July 2020; accepted in revised form 15 February 2021. Available online 22 March 2021